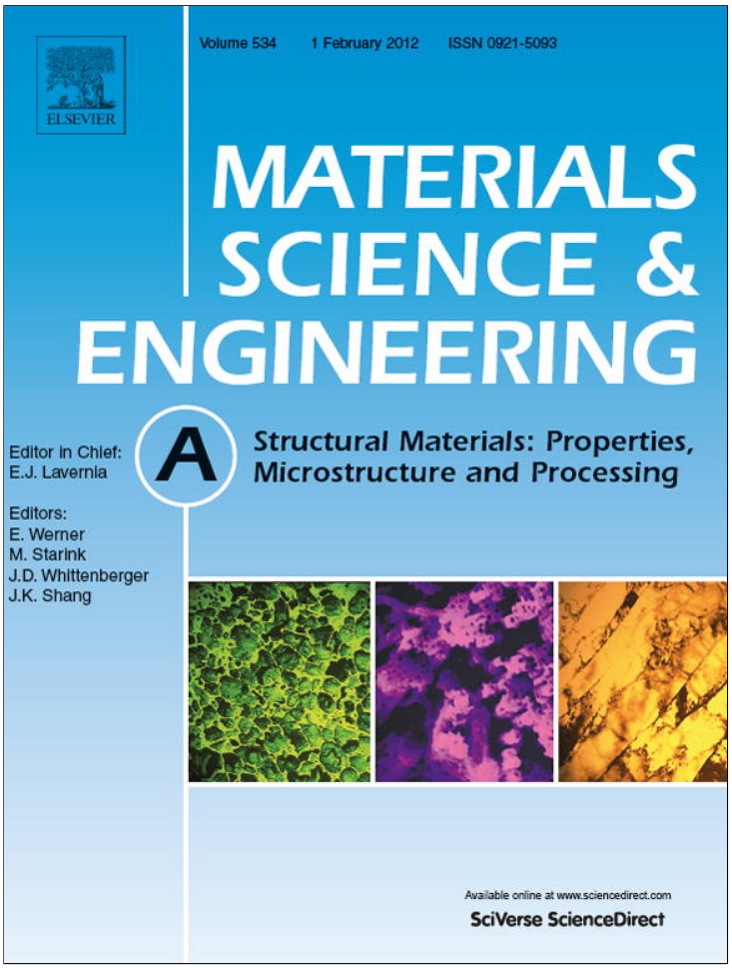

Materials Science and Engineering A 534 (2012) 1–6

Contents lists available at SciVerse ScienceDirect

Materials Science and Engineering A

journal homepage: www.elsevier.com/locate/msea

Precipitation microstructure and age-hardening response of an Mg–Gd–Nd–Zn–Zr alloy

J.H. Li[a,c,1], G. Sha[a,b,*], T.Y. Wang[a], W.Q. Jie[c], S.P. Ringer[a,b]

[a] Australian Centre for Microscopy and Microanalysis, The University of Sydney, Madsen Building F09, Sydney, NSW 2006, Australia
[b] ARC Centre of Excellence for Design in Light Metals, The University of Sydney, Sydney, NSW 2006, Australia
[c] State Key Laboratory of Solidification Processing, Northwestern Polytechnical University, Xi'an, 710072, China

ARTICLE INFO

Article history:
Received 14 December 2010
Received in revised form 11 June 2011
Accepted 25 October 2011
Available online 3 November 2011

Keywords:
Magnesium alloys
Precipitation
Age hardening
Atom probe tomography
Transmission electron microscopy

ABSTRACT

Precipitates in an Mg–3.6Gd–2.8Nd–0.6Zn–0.4Zr (wt.%) alloy aged for times up to 70 h at 200 °C have been characterised using transmission electron microscopy and atom probe tomography. The precipitate phases known as β″, β′ and β_1 occur during this ageing. The solute elements Nd, Zn and Gd partition significantly into these precipitates. The enhanced ageing hardening response after aged 70 h is mainly attributed to the precipitation of β′ and β_1 with a number density by a factor of 10 less than that of β″ and β′ precipitates formed after 3 h ageing.

1. Introduction

Magnesium alloys are attractive due to their specific strength, providing potential for weight reduction in automotive and aerospace applications [1,2]. The Mg–Nd based alloys such as ZM-6 in China and ML10 in Russia exhibit a strong age hardening response and have been used in various structural airframe components. However, the high temperature mechanical properties of these and other Mg–Nd based alloys are inadequate for technological applications above temperatures of 250 °C. The development of Mg alloys for these higher temperature applications remains a significant research target for the international materials community [3–18] and this is also the general subject of this contribution.

Heavy rare earth (HRE) elements such as Nd, Gd, Y, Dy, Er, Sc, Tb and Sm, have been used widely to improve the mechanical properties of Mg alloys at both room and elevated temperatures [3–12]. Indeed, most high-strength Mg alloys such as WE54/43 and QE22 contain HRE elements. The level of alloying addition of the HRE elements is a critical concern in alloy development and design because of both material costs and the desire to have the alloy as light as possible. This has driven significant research in recent times: (e.g.) Nie at al. [17] have demonstrated that small additions of Zn stimulate an age hardening response in Mg–Gd alloys that possess Gd contents that are below the level ordinarily associated with a significant ageing response. Moreover, combined additions of Gd with Zn to Mg–Nd alloys have been reported to improve the mechanical properties of the alloys, particularly at elevated temperatures [11,12]. It is expected that the improvement of mechanical properties of these Mg–Gd–Nd–Zn alloys should be correlated to the precipitates microstructures formed during ageing treatment. To date, there is a lack of detailed investigations to reveal the evolution of precipitates microstructure and the partitioning of solutes during ageing these alloys.

In this paper, transmission electron microscopy (TEM) and atom probe tomography (APT) have been employed to characterise precipitates microstructures formed during ageing a quinary Mg–3.6Gd–2.8Nd–0.6Zn–0.4Zr (wt.%) alloy. Quantitative APT analysis aims to reveal the partitioning behaviour of solutes. Comprehensive structural information obtained from a combination of TEM and APT characterisations will help to elucidate the precipitation reactions and to understand the nanostructure providing hardening effect in the alloy.

2. Experimental procedures

The Mg–3.6Gd–2.8Nd–0.6Zn–0.4Zr (wt.%) alloy was prepared from pure Mg (99.9%), Zn (99.9%), Nd (99.9%), Mg–28Gd and

* Corresponding author at: Australian Centre for Microscopy and Microanalysis, The University of Sydney, Madsen Building F09, Sydney, NSW 2006, Australia. Tel.: +61 2 90369050; fax: +61 2 93517682.
E-mail addresses: jie-hua.li@hotmail.com (J.H. Li), gang.sha@sydney.edu.au (G. Sha).
[1] Current address: Chair of Casting Research, the University of Leoben, Austria.

0921-5093/$ – see front matter.
doi:10.1016/j.msea.2011.10.092

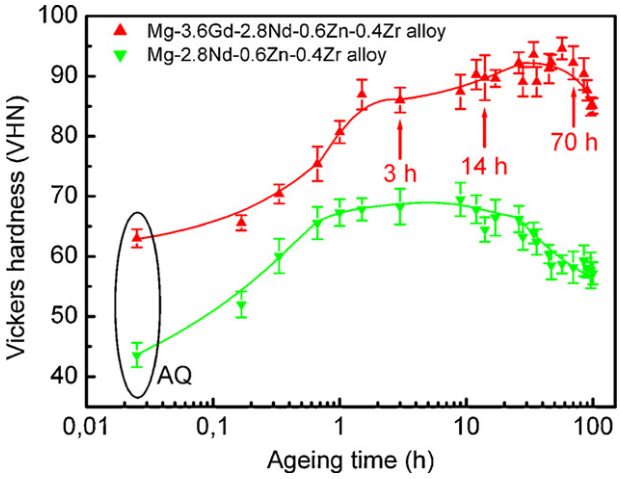

Fig. 1. Age hardening response of Mg–3.6Gd–2.8Nd–0.6Zn–0.4Zr (wt.%) alloy aged at 200 °C. For comparison, the result of the Gd-free alloy is also included.

Mg–33Zr (wt.%) master alloys in an electric resistance furnace under the protection of an anti-oxidizing flux, and then cast into a sand mould. Solution treatment was performed in a salt bath at 520 °C for 18 h, followed by quenching into cold water and then ageing in oil at 200 °C for up to 100 h. Vickers hardness testing was performed using a LECO Hardness Tester (LV700AT) with 10 N load and 15 s dwell time. Each data point reported in Fig. 1 represents an average of at least 10 measurements. The foil specimens for TEM were prepared by twin jet electro-polishing in a solution of 25% $HClO_4$ and 75% methanol cooled down to −40 °C with a voltage of 20 V, and then using low energy beam ion thinning for surface cleanness. TEM examinations were performed using a CM12 operating at 120 kV and a JEOL-3000F operating at 300 kV. The samples for atom probe analysis were cut and mechanically ground to square rods of approximately 0.5 mm × 0.5 mm × 15 mm, and then sharpened by micro-electro-polishing. APT analyses were performed using an Imago LEAP^{TM} 3000 operating at a specimen temperature of 20 K, 20% pulse fraction and under ultrahigh vacuum conditions.

Atom probe data sets were carefully reconstructed using an approach outlined recently by Gault and co-workers [19]. The maximum separation algorithm was employed to identify solute-rich precipitates and the concentration of the matrix was measured after removing identified precipitates [20,21]. Nd, Gd and Zn were selected as precipitation solutes and a separation distance of 0.8 nm and the minimum size of 15 solute atoms were used in the precipitate identification [22]. A selection box analysis method was used to measure precipitate composition. Such methods can convolute non-systematic errors where irregular morphologies are involved. Selection box methods also tend to minimise the influence of ion trajectory overlaps that can occur in multi-component systems such as here, where elements with widely varying evaporative fields are involved. The average composition of precipitates was measured from their central 2 nm region.

3. Results and discussion

3.1. Age hardening response of the Mg–Gd–Nd–Zn–Zr alloy

Fig. 1 reveals the age hardening response of the quinary Mg–3.6Gd–2.8Nd–0.6Zn–0.4Zr (wt.%) alloy. For comparison, the result of the Gd-free alloy is also included. It is clear that the age hardening response of the alloy containing 3.6 wt% Gd is higher than that of Gd-free alloy. It should be noted that the hardness of the quinary alloy increased quickly during the first 1.5 h at 200 °C, with a hardness increase from 65 HV of an as-quenched sample to 85 HV of a sample aged for 1.5 h. The 20 HV hardness increment is equivalent to 30% of the initial hardness of the as-quenched sample. This fast age-hardening response can be directly correlated to the stronger partitioning of Nd in Mg–Nd based alloys [13]. Then it reached a plateau-like range before reaching peak hardness after 70 h. Further ageing led to over-ageing and a progressive decrease in hardness. On the basis of these results, the samples aged at 0 h (as-quench), 3 h, 14 h and 70 h were selected for TEM observation and APT analysis.

3.2. TEM characterisation of precipitates in the Mg–Gd–Nd–Zn–Zr alloy

Fig. 2 shows a typical bright field (BF) TEM image and the corresponding selected area electron diffraction (SAED) pattern and energy dispersive X-ray (EDX) spectra taken from the as-quench Mg–3.6Gd–2.8Nd–0.6Zn–0.4Zr (wt.%) alloy. Only some particles containing Zr (Fig. 2c) are rarely distributed in the α-Mg matrix. No other precipitates are present in the microstructure (Fig. 2a and b). These Zr particles were believed to play an important role in the grain refinement of Mg alloy, but have no great effect on the precipitation strengthening due to their sparse distribution.

Fig. 3 shows a series of representative $[0\,1\,\bar{1}\,0]_{Mg}$ BF TEM images and the corresponding SAED patterns of samples aged at 200 °C for 3 h, 14 h and 70 h. Notwithstanding the well-known difficulties in achieving large, uniformly thin regions of foil in Mg alloys containing multiple HREs, this microscopy confirms the presence of a fine and uniform dispersion of precipitates in all of these ageing conditions. After ageing for 3 h, the SAED pattern in $[0\,1\,\bar{1}\,0]_{Mg}$ zone axis of the Mg matrix, as shown in Fig. 3b, was observed containing the weak diffraction streaks at $1/2(2\,\bar{1}\,\bar{1}\,0)_{Mg}$ and $1/2(2\,\bar{1}\,\bar{1}\,4)_{Mg}$ (marked with a white arrow), indicating that β″ precipitates formed in the alloy. The β″ phase possesses a DO_{19} crystal structure with a hexagonal unit cell of $a = b = 0.64$ nm and $c = 0.52$ nm [8] and it was reported to have a stoichiometry Mg_3X [10]. The β″ precipitates have a general habit plane parallel to $\{2\,\bar{1}\,\bar{1}\,0\}_{Mg}$. In addition to those weak diffraction streaks of β″ precipitates, the extremely weak diffraction of β′ precipitates at $1/2(2\,\bar{1}\,\bar{1}\,2)_{Mg}$, marked with a black arrow in Fig. 3b, was observed in the $[0\,1\,\bar{1}\,0]_{Mg}$ SAED pattern. This suggests that a low number density of β′ precipitates co-exist with the more numerous β″ precipitates at this stage of ageing. The β′ phase is known to have a base-centred orthorhombic unit cell $a = 0.640$ nm, $b = 2.223$ nm, $c = 0.521$ nm [8] and stoichiometry Mg_5X [10].

After ageing for 14 h, diffraction intensity at $1/2(2\,\bar{1}\,\bar{1}\,2)_{Mg}$ was stronger in the $[0\,1\,\bar{1}\,0]_{Mg}$ SAED patterns (marked with a black arrow in Fig. 3d), suggesting that more β′ precipitates formed. After ageing for 70 h, a weak diffraction spot clearly adjacent to $1/2(2\,\bar{1}\,\bar{1}\,0)_{Mg}$, as marked with a black box in Fig. 3f, indicates the presence of β_1 in the microstructure. This phase possesses a face-centred cubic unit cell with $a = 0.72$ nm and stoichiometry of Mg_3X [6,8,10]. The orientation relationships between the precipitates such as β″, β′, β_1 and the matrix are in agreement with those reported previously [6,8,10]. Thus, the precipitation sequence in this quinary Mg alloy during ageing is supersaturated solid solution (SSSS) → β″ (DO_{19}) → β′ (bco) → β_1 (fcc). β phase (a face-centred cubic unit cell with $a = 2.223$ nm and stoichiometry of Mg_3X [6]) has been considered to the equilibrium phase in the alloy, it may eventually precipitate, although it was not observed over 70 h ageing at 200 °C.

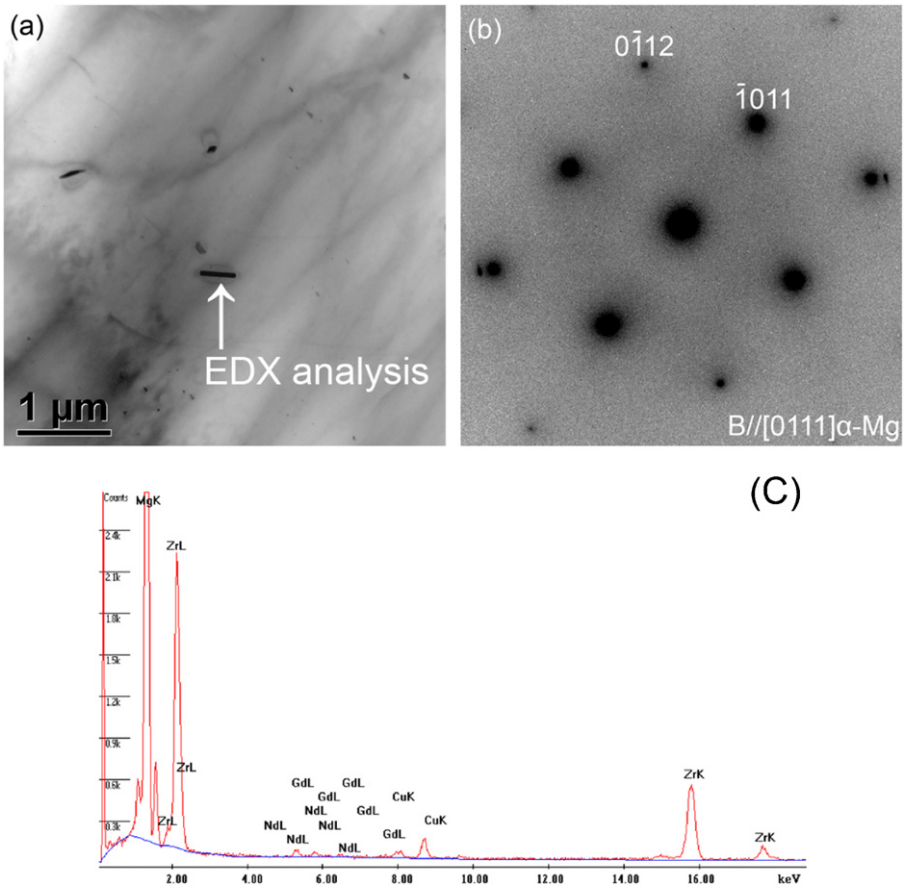

Fig. 2. TEM bright field image (a), corresponding SAED pattern (b) and EDX analysis (c) taken from the as-quench Mg–3.6Gd–2.8Nd–0.6Zn–0.4Zr (wt.%) alloy.

3.3. APT characterisation of precipitates in the Mg–Gd–Nd–Zn–Zr alloy

Fig. 4 provides a series of three-dimensional atom maps recorded from atom probe experiments on specimens of the Mg–3.6Gd–2.8Nd–0.6Zn–0.4Zr (wt.%) alloy after ageing at 200 °C for (a) 3 h (b) 14 h and (c) 70 h. It is clear that all three of the main solute elements, Nd, Gd and Zn were directly imaged within the precipitates. Using the zone lines and poles observed from the field desorption image available in atom probe microscopy, the view directions of the tomograms provided can be specifically defined, e.g. the view direction of images in Fig. 4a–c is $[0\,0\,0\,1]_{Mg}$. By examining a small regime marked with white solid lines in Fig. 4a at a high magnification, atomic planes $(0\,1\,\bar{1}\,0)_{Mg}$ and $(0\,1\,\bar{1}\,1)_{Mg}$ were clearly resolved in Figs. 5a and b. Three elongated precipitates are present in the small volume. A platelet precipitate habiting on $\{0\,1\,\bar{1}\,0\}_{Mg}$ is probably β′. This suggestion is consistent with the habit plane $\{0\,1\,\bar{1}\,0\}_{Mg}$ of β′ in Mg alloys reported in literatures [16,18]. A rod precipitate habiting on $\{\bar{2}\,1\,1\,0\}_{Mg}$ only separated by one or two atomic planes from the β′ platelet may be identified as β″, as seen in Fig. 5b. By examining the precipitates from different view directions, we found that most precipitates were elongated with their longitudinal axis parallel to $[0\,0\,0\,1]_{Mg}$. This observation is in agreement with previous TEM observations for β″, β′ and β_1 [6,10].

From the $[0\,0\,0\,1]_{Mg}$ view direction, the size of large precipitates was found to increase with ageing time (Fig. 4), which is not easy to see from the whole analysed volume due to the overlap of the high number density of precipitates (Fig. 4b). Most of the precipitates formed between 3 h and 70 h ageing have elongated morphology along $[0\,0\,0\,1]_{Mg}$, which are effective obstacles to basal slip [23]. It is also noteworthy that the number density of precipitates appears to be highest in the sample aged 3 h and that this progressively decreases when compared to the number densities of precipitates after ageing for 14 h and 70 h. Our analysis of total number density reveals that there are less precipitates by a factor of 10 in the sample aged 70 h at 200 °C compared to the sample aged 3 h and yet the hardness is 10% higher in the 70 h sample. The decrease in precipitate number density is in contrast to an increase in hardness with increasing ageing time from 3 h to 70 h, probably implying that the different precipitates formed under different ageing time had the different potency in producing strengthening effect. Given that the formation of more β′ and β_1 precipitates with the increase of ageing time as revealed by TEM characterisation described previously, we can conclude that the β′ and β_1 are more potent hardening obstacles than the β″ phase in the alloy. Interestingly, similar conclusion has been drawn in a few other Mg–RE alloys including WE54 alloy aged at 250 °C [6] and Mg–2.0Gd–1.2Y–1.0Zn–0.2Zr (at.%) alloy aged at 225 °C [10], where the peak-aged microstructure contains predominantly the β′ and β_1 phases.

The average compositions of large precipitates formed at different ageing time are shown in Fig. 6a. Since APT chemical composition analysis indicated that solute concentration increase with precipitate size, and TEM SAED analysis confirmed the co-existence of β″ and β′, β′ and β_1 in different ageing conditions, it is reasonable to assume here that large precipitate measured at 3 h should be corresponding to β′, and large high-solute-concentration precipitates observed at 70 h correspond to β_1. The Gd concentration within the large precipitates was effectively unchanged during

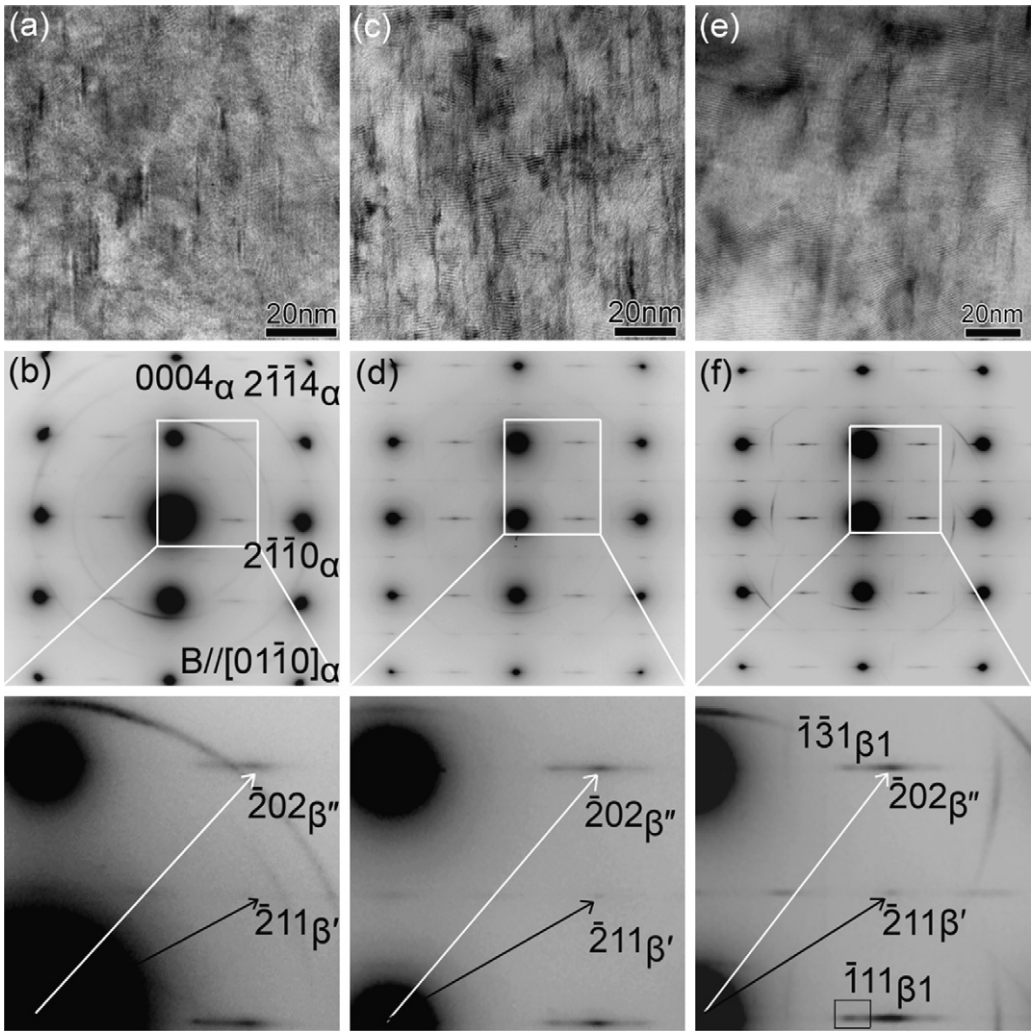

Fig. 3. $[0\,1\,\bar{1}\,0]_{Mg}$ bright field TEM images and corresponding SAED patterns from the microstructure of Mg–3.6Gd–2.8Nd–0.6Zn–0.4Zr (wt.%) alloy samples aged at 200 °C for various times: (a and b) 3 h, (c and d) 14 h and (e and f) 70 h.

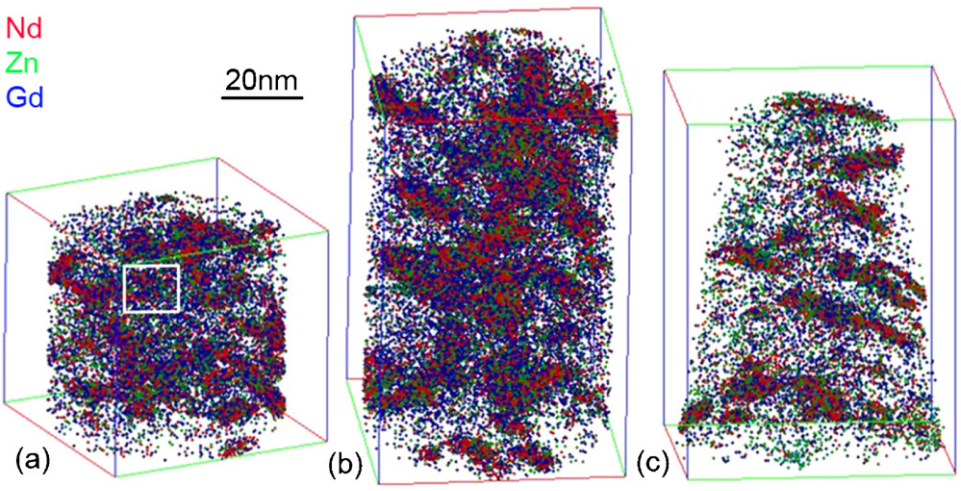

Fig. 4. Combined atom maps of Nd (red), Gd (blue) and Zn (green) obtained from Mg–3.6Gd–2.8Nd–0.6Zn–0.4Zr (wt.%) alloy samples aged at 200 °C for (a) 3 h, (b)14 h and (c) 70 h, in a view direction close to the $[0\,0\,0\,1]_{Mg}$ zone axis. (For interpretation of the references to color in this figure legend, the reader is referred to the web version of the article.)

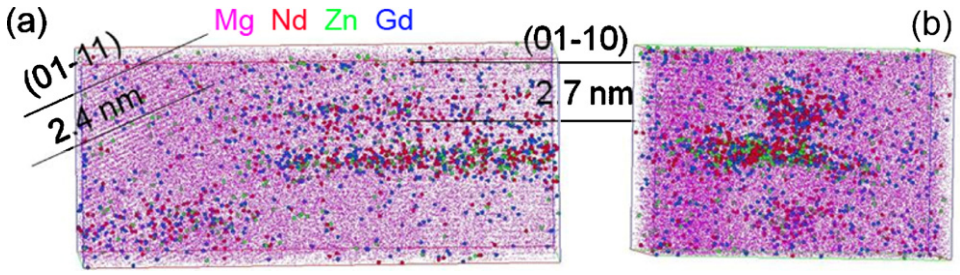

Fig. 5. High resolution images of a small region (as marked with white solid lines in Fig. 3a) obtained from Mg–3.6Gd–2.8Nd–0.6Zn–0.4Zr (wt.%) alloy samples aged at 200 °C for 3 h, in view directions close to $[\bar{2}\,1\,1\,0]_{Mg}$ (a) and $[0\,0\,0\,1]_{Mg}$ (b) zone axes respectively.

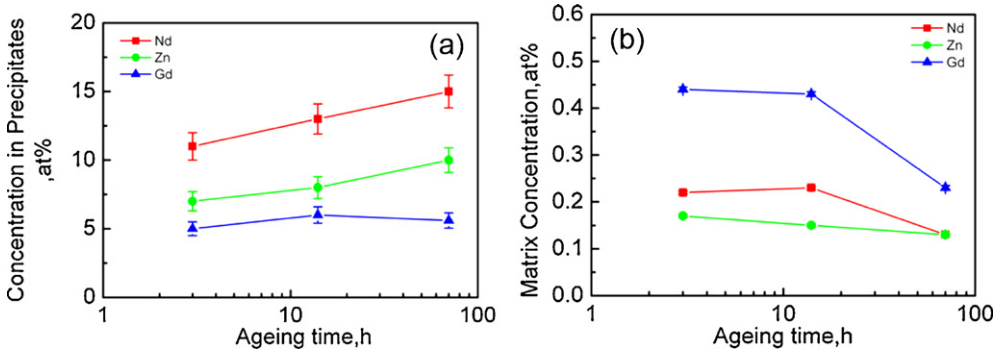

Fig. 6. Solute concentrations of large precipitates (a) and matrix (b) in Mg–3.6Gd–2.8Nd–0.6Zn–0.4Zr (wt.%) alloy samples aged at 200 °C from 3 h to 70 h.

70 h of ageing at 200 °C. However, the Zn and Nd concentrations within the precipitates increased with increasing ageing time. The Nd:Zn ratio of the precipitates was approximately 1.6:1 throughout the ageing sequence examined here, which is similar to, though slightly less than the 2:1 ratio reported from TEM-based energy dispersive X-ray spectroscopy (EDXS) microanalysis of β′ precipitates in a similar alloy [16]. The precipitates were richest in Nd of all solutes and the concentration of this element increased from ~11 to ~15 at.% during ageing. This is also close to the average composition of 15 at.% measured by EDXS [16]. A combined concentration of Mg and Zn is 84 at.%, and a combined concentration of Nd and Gd is 16 at.% in large precipitates (likely β′) formed after ageing for 3 h. This gives the large precipitates with a stoichimetry of $(Mg, Zn)_5(Nd, Gd)$. The stoichimetry is consistent with β′ having Mg_5Nd reported in binary Mg–Nd alloy [13]. In contrast, the composition of the large precipitates formed after ageing for 70 h that were thought to be β_1 phase on the basis of the SAED analysis, Fig. 3, gives $(Mg, Zn)_4(Nd, Gd)$. This is in contrast with Mg_3X proposed by previous research [6,8,10]. Further APT investigation is necessary to measure the chemistry of β_1 in over-aged sample. It has been reported that the precipitates formed in binary Mg–Nd alloys possess a range of compositions from Mg_5Nd to Mg_9Nd [16,18]. We conclude that the transformations from β″ to β′ and β_1 are related to further enrichment of Nd, Zn and Gd solutes in the precipitates. The solute concentrations in the matrix decreased during ageing at 200 °C from 3 h to 70 h, as indicated in Fig. 6b. These results indicate that significant solutes have partitioned into the precipitates. The low concentrations of Nd, Gd and Zn measured in the matrix after ageing for 70 h indicate that the equilibrium solubility of Nd should be less than 0.13 at.% in this Mg alloy and that the solubility of Gd should be lower than 0.23 at.%. This may explain why Gd does not seem to partition into any of the β″, β′, or β_1 precipitates phases observed in these low Gd content alloys [16].

4. Conclusion

The precipitate sequence in the Mg–3.6Gd–2.8Nd–0.6Zn–0.4Zr (wt.%) alloy during ageing at 200 °C over 70 h is $\beta'' \rightarrow \beta' \rightarrow \beta_1$. The precipitates have a lamella-like morphology with a longitudinal axis parallel to $[0\,0\,0\,1]_{Mg}$. The solute elements Nd, Zn and Gd partition significantly into the precipitates (β″, β′ and β_1). The peak hardness at 70 h is in coincidence with a low number density of precipitates (β′ and β_1) in the microstructure of the alloy but with a high fraction of the total solutes associated with precipitation. The enhanced ageing hardening response after aged 70 h was mainly attributed to the precipitation of β′ and β_1 precipitates with a number density by a factor of 10 less than that of β″ and β′ precipitates formed after 3 h ageing.

Acknowledgments

The authors are grateful for scientific and technical input and support from the Australian Microscopy & Microanalysis Research Facility (AMMRF) node at the University of Sydney. J.H. Li also wishes to thank the China Scholarship Council for financial support. This work is partly supported by the Doctorate Foundation of Northwestern Polytechnical University under grant no. (CX200705).

References

[1] B. Smola, I. Stulíková, F. von Buch, B.L. Mordike, Mater. Sci. Eng. A 324 (2002) 113–117.
[2] J. Grobner, R. Schmid-Fetzer, J. Alloys Compd. 320 (2001) 296–301.
[3] S.M. He, X.Q. Zeng, L.M. Peng, X. Gao, J.F. Nie, W.J. Ding, J. Alloys Compd. 427 (2007) 316–323.
[4] B.L. Mordike, Mater. Sci. Eng. A 324 (2002) 103–112.
[5] V. Neubert, I. Stulíková, B. Smola, B.L. Mordike, M. Vlanch, A. Bakkar, J. Pelcová, Mater. Sci. Eng. A 462 (2007) 329–333.

[6] J.F. Nie, B.C. Muddle, Acta Mater. 48 (2000) 1691–1703.
[7] I. Stulikova, B. Smoloa, B.L. Mordike, Phys. Status Solidi A 190 (2002) 5–7.
[8] T. Honma, T. Ohkubo, K. Hona, S. Kamado, Mater. Sci. Eng. A 395 (2005) 301–306.
[9] J.H. Li, W.Q. Jie, G.Y. Yang, Acta Metall. Sinca 10 (2007) 1077–1081.
[10] T. Honma, T. Ohkubo, S. Kamado, K. Hono, Acta Mater. 55 (2007) 4137–4150.
[11] J.H. Li, W.Q. Jie, G.Y. Yang, Trans. Nonferrous Met. Soc. China 18 (2008) s27–s32.
[12] J.H. Li, W.Q. Jie, G.Y. Yang, Rare Met. Mater. Eng. 37 (2008) 1751–1754.
[13] T.J. Pike, B. Noble, J. Less Common Met. 30 (1973) 63.
[14] P.A. Nuttall, T.J. Pike, B. Noble, Metallography 13 (1980) 3.
[15] R. Wilson, C.J. Bettles, B.C. Muddle, J.F. Nie, Mater. Sci. Forum 419–422 (2003) 267–272.
[16] L.R. Gill, G.W. Lorimer, P. Lyon, Adv. Eng. Mater. 9 (2007) 784–792.
[17] J.F. Nie, X. Gao, S.M. Zhu, Scr. Mater. 53 (2005) 1049–1053.
[18] P.J. Apps, H. Karimzadeh, J.F. King, G.W. Lorimer, Scr. Mater. 48 (2003) 1023–1028.
[19] M.P. Moody, B. Gault, L.T. Stephenson, D. Haniel, S.P. Ringer, Ultramicroscopy 109 (2009) 815–824.
[20] J.M. Hyde, C.A. English, Microstructural processes in irradiated materials, in: R.G.E. Lucas, L. Snead, M.A.J. Kirk, R.G. Elliman (Eds.), MRS 2000 Fall Meeting Symposium, Boston, MA, 2001, p. 27.
[21] D. Vaumousse, A. Cerezo, P.J. Warren, Ultramicroscopy 95 (2003) 215.
[22] G. Sha, J.H. Li, W.Q. Jie, S.P. Ringer, in: K.U. Kainer (Ed.), Proceedings of 8th International Conference on Magnesium Alloys and their Applications, Wiley-VCH Verlag GmbH & Co. KGaA, Weinheim, 2009, pp. 40–46.
[23] J.F. Nie, Scr. Mater. 48 (2003) 1009–1015.